NAVIER-STOKES CALCULATIONS FOR A COMPLETE AIRCRAFT

Reijo Lehtimäki* Seppo Laine† Timo Siikonen‡ Esa Salminen§

Helsinki University of Technology, FIN-02150 Espoo, Finland

Abstract

The present study deals with the Navier-Stokes calculations for a flow past a jet trainer (BAe Hawk). An important and difficult part of the work has been to generate a good grid around the aircraft. To facilitate the grid generation the computation domain has been divided into 14 blocks. The numerical method used to solve the Reynolds-averaged Navier-Stokes equations is a finite-volume method which utilizes upwind differencing and a DDADI-factorized implicit time integration. Two different turbulence models are employed, an algebraic model and a low-Reynolds number $k-\epsilon$ model. Results are given for a case: $Ma = 0.45$, $Re = 18.6 \times 10^6$, and $\alpha = 3°$. They are compared with a solution obtained with a panel method.

Nomenclature

C_D	drag coefficient, drag/$q_\infty S$
C_L	lift coefficient, lift/$q_\infty S$
C_{d_p}	pressure drag coefficient
C_m	pitching moment coefficient based on $\bar{c}$
C_p	pressure coefficient, $(p - p_\infty)/q_\infty$
Ma	freestream Mach number
Re	Reynolds number based on $\bar{c}$
S	area of reference wing planform (16.69 m^2)
V_∞	freestream velocity
$\bar{c}$	wing mean aerodynamic chord (1.777 m)
c_f	local skin friction coefficient based on q_∞
c_l	local lift coefficient
p_∞	freestream pressure
q_∞	freestream kinetic pressure, $0.5\rho_\infty V_\infty^2$
y/s	fraction of semispan
α	angle of attack, deg
ρ_∞	freestream density

*Research Scientist, Laboratory of Aerodynamics
†Head of the Laboratory of Aerodynamics
‡Associate Professor, Laboratory of Applied Thermodynamics
§Research Scientist, Laboratory of Applied Thermodynamics

Introduction

In recent years, CFD has been utilized for aircraft aerodynamics. Most of the applications have concerned inviscid calculations, i.e. Euler solutions, see e.g. (1). Viscous solutions have mainly been determined for wings alone or for simple wing-body combinations. Only a few viscous results have been published for a complete aircraft e.g. (2), the reason being that viscous solutions require a huge number of grid points and a great deal of computer time to be accurate enough.

The present study describes calculation of viscous flow past a jet trainer (BAe Hawk) by means of a Reynolds-averaged Navier-Stokes solver, FINFLO. The FINFLO code, developed in the Laboratory of Aerodynamics at the Helsinki University of Technology, uses a finite-volume approach; see Refs. (3), (4) and (5). The inviscid part of the flux on the cell surface is computed by solving approximately a locally one-dimensional Riemann problem.(6) The viscous terms are evaluated utilizing thin-layer approximation. The discretized equations are integrated in time by applying DDADI-factorization.(7) A multigrid technique is employed to speed up the convergence. Several different turbulence models can be applied: algebraic and low-Reynolds number two equation models.

The present calculations were done in order to test the code for a realistic aircraft application. Certain details of the aircraft, such as the air intake, can be taken into account in the simulations. A very dense grid is therefore necessary. The generation of the grid is a complicated task, since C-type grids are used around the wing and tailplane in order to reduce the number of grid points. The grid, which consists of 4.3 million grid points around half the model, is dense enough to obtain sufficient refinement near the solid surface for the boundary layer flow and its interference with shock waves to be captured with sufficient accuracy. The grid is divided into fourteen blocks to facilitate grid generation, which has been carried out using algebraic and elliptic methods. In particular, the elliptic method presented in Ref. (8) has been applied in the blocks that are difficult to generate by means of an algebraic method.

Calculations have been performed with an algebraic Baldwin-Lomax turbulence model,(9) and Chien's low-

Reynolds number $k-\epsilon$ model.[10] Results will be given for chordwise pressure distributions, surface friction distributions, velocity distributions across the boundary layer, spanwise lift distribution, total lift, drag and pitching moment. For a comparison, the pressure distribution is also determined with a low-order panel method, presented in Ref. (11).

Numerical Method

Viscous Calculations

Governing Equations. The Reynolds averaged Navier–Stokes equations and the equations for the the kinetic energy k and dissipation ϵ of turbulence can be written in the following form

$$\frac{\partial U}{\partial t}+\frac{\partial(F-F_v)}{\partial x}+\frac{\partial(G-G_v)}{\partial y}+\frac{\partial(H-H_v)}{\partial z}=Q \quad (1)$$

where $U=(\rho,\ \rho u,\ \rho v,\ \rho w,\ E,\ \rho k,\ \rho\epsilon)^T$. Here ρ is the density; the velocity is $\vec{V}=u\vec{i}+v\vec{j}+w\vec{k}$; p is the pressure, and E the total internal energy defined as

$$E=\rho e+\frac{\rho\vec{V}\cdot\vec{V}}{2}+\rho k \quad (2)$$

where e is the internal energy. The pressure is calculated from the perfect gas law

$$p=(\gamma-1)\rho e \quad (3)$$

where γ is the ratio of specific heats c_p/c_v. The source term Q has non-zero components, which will be given later, only for turbulence equations. For the Reynolds stresses, we apply Boussinesq's approximation

$$-\rho u_i''u_j''=\mu_T[\frac{\partial u_j}{\partial x_i}+\frac{\partial u_i}{\partial x_j}-\frac{2}{3}(\nabla\cdot\vec{V})\delta_{ij}]-\frac{2}{3}\rho k\delta_{ij} \quad (4)$$

where μ_T is a turbulent viscosity coefficient. The molecular viscosity is calculated from Sutherland's formula. In the $k-\epsilon$ model the turbulent viscosity is calculated from

$$\mu_T=c_\mu\frac{\rho k^2}{\epsilon} \quad (5)$$

Source Term. Near the wall the low-Reynolds number model proposed by Chien[10] is adopted. The source term for Chien's model is given as

$$Q=\begin{pmatrix} P-\rho\epsilon-2\mu\dfrac{k}{y_n^2} \\ c_1\dfrac{\epsilon}{k}P-c_2\dfrac{\rho\epsilon^2}{k}-2\mu\dfrac{\epsilon}{y_n^2}e^{-y^+/2}\end{pmatrix} \quad (6)$$

where y_n is the normal distance from the wall, and y^+ is defined by

$$y^+=y_n\left[\frac{\rho|\nabla\times\vec{V}|}{\mu}\right]_w^{1/2} \quad (7)$$

The production of turbulent kinetic energy is modelled using Reynolds stresses obtained from Eq. 4

$$P=-\rho u_i''u_j''\frac{\partial u_i}{\partial x_j}$$
$$=[\mu_T(\frac{\partial u_i}{\partial x_j}+\frac{\partial u_j}{\partial x_i}-\frac{2}{3}\delta_{ij}\frac{\partial u_k}{\partial x_k})-\frac{2}{3}\delta_{ij}\rho k]\frac{\partial u_i}{\partial x_j} \quad (8)$$

Spatial Discretization. For the solution, a finite-volume technique is applied. The finite volume formulation is obtained by integrating the differential equations over a computational cell i

$$V_i\frac{dU_i}{dt}=\sum_{faces}-S\hat{F}+V_iQ_i \quad (9)$$

where the sum is taken over the faces of the computational cell. The flux for the face is defined as

$$\hat{F}=n_x(F-F_v)+n_y(G-G_v)+n_z(H-H_v) \quad (10)$$

In the evaluation of the inviscid fluxes, Roe's method[6] is applied. The flux is calculated as

$$\hat{F}=T^{-1}F(TU) \quad (11)$$

where T is a rotation matrix which transforms the dependent variables to a local coordinate system normal to the cell surface. In this way only the Cartesian form F of the flux is needed.

Boundary Conditions. At the free-stream boundary the values of the dependent variables are kept as constants. In the flowfield, k and ϵ are limited from below to their free-stream values. In the calculation of the inviscid fluxes at the solid boundary, flux-difference splitting is not used. Since the convective speed is equal to zero on the solid surfaces, the only contribution to the inviscid surface fluxes arises from the pressure terms in the momentum equations. A second-order extrapolation is applied for the evaluation of the wall pressure.

The viscous fluxes on the solid surfaces are obtained by setting $u=v=w=0$ on the wall. The central expression of the viscous terms is replaced by a second-order one-sided formula. The wall temperature is set to the free-stream stagnation temperature. The viscous fluxes of k and ϵ are also set to zero at the wall.

Solution Algorithm. The discretized equations are integrated in time by applying the DDADI-factorization.[7] This is based on the approximate factorization and on the splitting of the Jacobians of the flux terms. The resulting implicit stage consists of a backward and forward sweep in every coordinate direction.

The sweeps are based on a first-order upwind differencing. In addition, the linearization of the source term is factored out of the spatial sweeps. The boundary conditions are treated explicitly, and a spatially varying time step is utilized. For a more thorough description of the solution method applied, see Refs. (3), (4) and (5).

Inviscid Calculations

The inviscid calculations were performed with a low-order panel method, Ref. (11). The method uses constant source-distribution on the surface panels and horseshoe vortices on the mean surface of the wing. The lift of the fuselage is taken into account by generating horseshoe vortices inside the fuselage and applying kinematic flow condition inside the fuselage. The compressibility effects are taken into account by using a modified form of the Göthert rule, whereby the boundary condition is satisfied on the real body.

Grid Generation

Both the calculations, the viscous as well as the inviscid, need a suitable grid. As a coarse surface panel model is sufficient for the inviscid calculations, a dense three-dimensional volume grid is required to solve the Navier-Stokes equations.

The surface patch definition of the complete BAe Hawk aircraft was obtained in the IGES format. This data was employed to extract a high-density surface grid definition, which was then used to generate a coarser surface grid for the Navier-Stokes computation. Some minor details, like boundary layer fences or dorsal fins, were excluded in the calculation model. The number of elements in the surface grid for the viscous calculation is 38,400. The surface grid is depicted in Fig. 1. The panel model was generated utilizing relatively coarse surface node point data, which was written out directly from a CAD program.

A structured multiblock grid is used in the viscous calculations. The grid has to be dense enough ($y^+ \approx 1$) on the aircraft surface in order to resolve the viscous boundary layer. Furthermore, the grid has to be extended to a sufficient distance from the body to justify the assumption of the free-stream boundary condition. The limiting factor is the number of grid cells that could be used. The CPU time required for the flow calculation would increase with the number of grid cells used. However, the absolute upper limit for the grid size was set by the available 2 Gb main memory size of the Silicon Graphics Power Challenge computer used for the flow calculations. Typically, 6 of the 12 processors available were used in both Navier-Stokes calculations. With the following block division the total number of grid cells in the half model became 4,306,944. In the $k-\epsilon$ model flow calculations some blocks were not used and the number of grid cells was only 4,202,496.

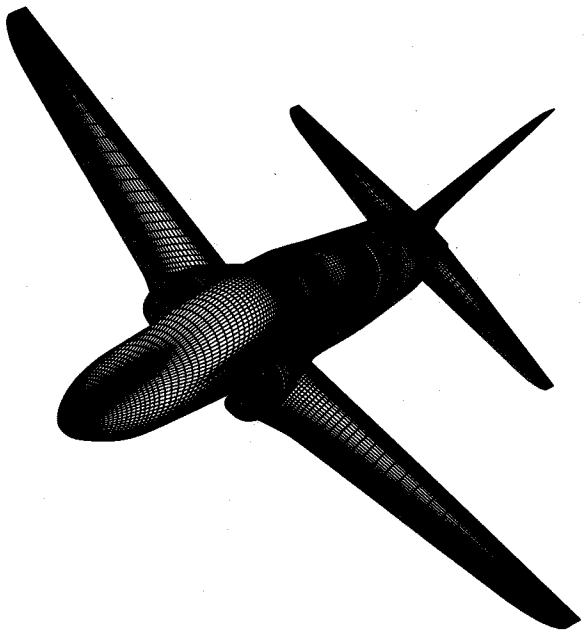

Figure 1. Surface grid of the BAe Hawk aircraft for the viscous calculation.

The grid extends to 30 m from the aircraft. The flow calculations with the $k-\epsilon$ turbulence model occupied 1.8 Gb of main memory.

For the wing-like bodies C-O type grid blocks were chosen in order to get a good resolution at the leading edge and to resolve the boundary layer without wasting too many cells in the farfield. When this choice is made, the rest of the block division falls into place quite naturally. The blocks around the wing and the stabilizers leave three gaps in the circumferential direction in between them, see Fig. 2. Each of these gaps is filled with a block. The upper and lower part of the aircraft forward of the wing was modeled with separate blocks. Due to some restrictions in the flow solver both of these blocks still had to be divided into three. The foremost part of the aircraft was generated as a single block to conserve grid cells. The front of the inlet is modeled as a separate block just to make the grid generation easier. Most of these blocks are of H-H type since that type of grid fits naturally with the surrounding blocks.

The concentrations of grid points that can be seen on the symmetry plane are due to similar concentrations on the fuselage. The surface grid is concentrated at the leading and the trailing edge of the wing and the stabilizers. These concentrations extend over the fuselage to the symmetry plane and continue to the farfield. This is, in fact, unnecessary and only tends to slow down the convergence of the flow solution.

The internal block boundaries were generated by simply drawing some lines from the body to the farfield and interpolating between them. This produced the somewhat unsmooth block boundaries seen in Fig. 2. The volume grid generation was mostly performed

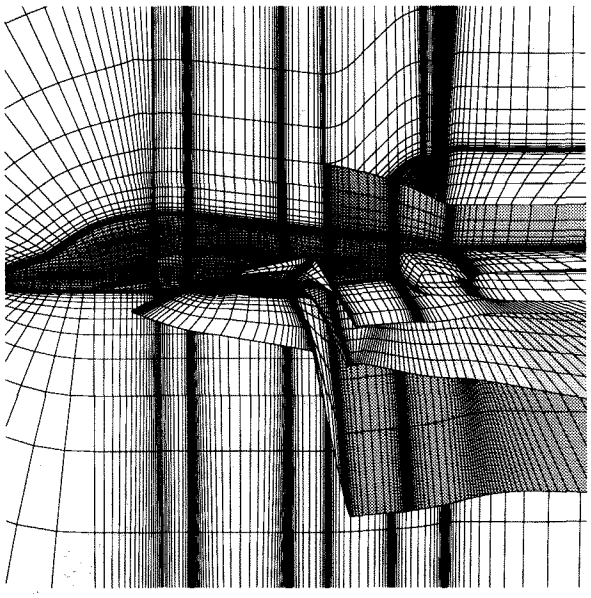

Figure 2. The block division of the volume grid. In addition to the surface of the aircraft, the symmetry-plane and parts of the outer surfaces of the blocks around the wing and the vertical and horizontal stabilizer are shown.

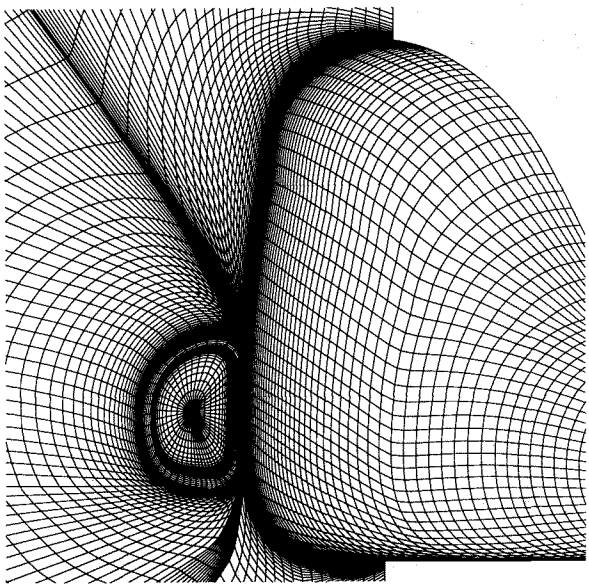

Figure 3. The grid around the inlet. The surface of the aircraft on the right and the outer surface of the inlet in the middle are cut by a cross-section of the grid. The cross section is composed of several coordinate surfaces belonging to different blocks of the multiblock grid.

with a standard transfinite interpolation utilizing multidimensional stretching functions. Some of the blocks are quite complex. For example, the block around the wing passes under the block around the horizontal stabilizer. This makes the upper boundary of the wing turn excessively, which then causes trouble when generating the volume grid for the block. The block around the horizontal stabilizer is for the same reason very narrow in the vertical direction, which, in fact, makes the gridding of that block non-trivial, too. Also the blocks ahead of the inlet were inverted after the transfinite interpolation. Whenever transfinite interpolation turned out to be inadequate, a method utilizing the Laplace system with stretching functions was used, see Ref. (8). A close-up view of the grid around the inlet is shown in Fig. 3.

Calculated Results

The flow past the BAe Hawk aircraft has been calculated for a case: $Ma = 0.45$, $Re = 18.6 \times 10^6$, $\alpha = 3°$. This case is computationally rather easy, since there is no flow separation or shock waves. Even an inviscid solution should give acceptable results for pressure distributions.

The results shown here concern a case without airflow through the air inlet. Therefore, the base of the aircraft is modelled with a sting with an inviscid surface. The lift, drag and pitching moment then include the influence of all other surfaces except the base and the air intake.

First, the Navier-Stokes solutions are described. In the outer boundary of the computation domain the free-stream values for pressure and velocity were prescribed. In the $k - \epsilon$ turbulence model calculations, the non-dimensional free-stream values of k and ϵ were 0.0002 and 0.1458, respectively. The quantity k was made non-dimensional with the square of the free-stream speed of sound and the quantity ϵ with the third power of the free-stream speed of sound and the reference length of $L_\infty = 1$ m. A multigrid technique with three multigrid levels was employed to speed up the convergence. In the direction normal to the surface a third-order accurate spatial discretation method was used, whereas in other directions a second-order method is utilized. When using the Baldwin-Lomax turbulence model, the flow was assumed to be turbulent on all surfaces. In the $k - \epsilon$ model the transition was allowed to occur by itself, which resulted in transition rather near the leading edges and the nose of the fuselage.

In order to get the calculations to converge, the Courant number had to be typically below 1, and therefore, the convergence speed was slower than normally. One reason for convergence problems might be the fact that the grid is very dense near the aircraft surface and at some block boundaries. Another reason might be that the grid density normal to the surface on the middle part of the fuselage was much too coarse. When employing the algebraic Baldwin-Lomax turbulence model, converged results were obtained after about seven thousand iterations. Fig. 4 shows convergence of lift, drag and the L_2-norm of the density residual for the B-L model. For the $k-\epsilon$ model, even 20,000 iterations were not enough. But this slow convergence probably results from defi-

Table 1. Calculated lift, pressure drag and pitching moment. Engine intake closed.

Method	B-L	$k-\epsilon$	panel
C_L	0.38	0.35	0.38
C_{D_p}	0.0092	0.014	0.009
C_m	-0.028	-0.039	-0.039

ciencies in the grid. Therefore, after having redesigned the block around the middle part of the fuselage, new calculations with the $k-\epsilon$ model will be carried out.

The results with the panel method were determined by using 1,717 panels for the half aircraft. For the lift generating surfaces 20 Kutta-panels were utilized.

Table 1 presents results for lift, pressure drag and pitching moment. The coefficients are based on the wing reference area 16.69 m^2 and the aerodynamic mean chord 1.777 m. The moment reference point lies at the 16.9 % position of the mean chord. As can be seen, the B-L model and the panel method produce quite similar results for lift and pressure drag. The $k-\epsilon$ model gives less lift and more pressure drag than the other two models.

Pressure distributions in the form of isobars on the aircraft surface can be seen in Fig. 5. The figure also includes results from the panel method calculations. The viscous and inviscid solutions agree quite well on the wing and tailplane, but there are differences on the fuselage.

Chordwise pressure distributions along the wing surface at five sections are depicted in Fig. 6 for the B-L model, the $k-\epsilon$ model and for the panel method. Again, the inviscid results agree quite well with the viscous solutions. (The wing cross-sections are curved and the y/s-values denote the position at the leading edge.)

The local lift coefficient distribution of the wing is presented in Fig. 7. The viscous solutions and the inviscid computation with the panel method yield very similar results. However, the viscous solutions give less lift along the wing than the panel method.

The next figures demonstrate viscous effects. Fig. 8 gives the local skin friction coefficient distribution along the wing surface at five sections. The coefficient is made dimensionless by dividing it by the free-stream kinetic pressure. The results of both turbulence models agree fairly well except very near the leading edge and near the wing root.

Fig. 9 depicts surface streamlines. The influence of the closed air intake is clearly seen to curve the flow on the fuselage surface near the intake.

Boundary layer profiles on the wing surface are shown in Fig. 10 in the form $u^+ = f(y^+)$ at a cross section $y/s = 0.45$. They indicate that the grid is dense enough near the surface since the y^+ value of the first cell is less than one. In the buffer layer the $k-\epsilon$ model yields lower velocities than the Baldwin-Lomax model, whereas in the logarithmic layer the opposite is true.

Conclusions

In this study the flow past a jet trainer has been calculated using a Navier-Stokes solver. The study has demonstrated the difficulty and importance of generating a good grid around a complex geometry. The generation of a structured grid requires much more human effort than any other part of the study. The viscous calculations agree quite well with each other and with an inviscid solution, since there is no flow separation or shocks. The low-Reynolds number $k-\epsilon$ model requires much more computational effort for a converged solution than the Baldwin-Lomax model. With the aid of new supercomputers, present studies are feasible and the Navier-Stokes flow solver a useful tool in aircraft design.

References

[1] C.-C. Rossow and H. Hoheisel, Numerical study of interference effects of wing-mounted advanced engine concepts. In *Proceedings of the 19th ICAS Congress*, pages 1272–1282, Anaheim, Sept. 1994. ICAS Paper 94-6.4.1.

[2] Y. M. Rizk and K. Gee, Unsteady simulation of viscous flowfield around F-18 aircraft at large incidence. *Journal of Aircraft*, 29(6):986–992, Nov.-Dec. 1992.

[3] T. Siikonen, J. Hoffren, and S. Laine, A multigrid *LU* factorization scheme for the thin-layer Navier–Stokes equations. In *Proceedings of the 17th ICAS Congress*, pages 2023–2034, Stockholm, Sept. 1990. ICAS Paper 90-6.10.3.

[4] T. Siikonen, P. Kaurinkoski, and S. Laine, Transonic flow over a delta wing using a $k-\epsilon$ turbulence model. In *Proceedings of the 19th ICAS Congress*, pages 700–710, Anaheim, Sept. 1994. ICAS Paper 94-2.3.2.

[5] T. Siikonen. An application of Roe's flux-difference splitting for the $k-\epsilon$ turbulence model, *International Journal for Numerical Methods in Fluids*, 21:1017–1039, 1995.

[6] P.L. Roe, Approximate Riemann solvers, parameter vectors, and difference schemes. *Journal of Computational Physics*, 43:357–372, 1981.

[7] C.K. Lombard, J. Bardina, E. Venkatapathy, and J. Oliger, Multi-dimensional formulation of CSCM — an upwind flux difference eigenvector split method for the compressible Navier–Stokes equations. In *6th AIAA Computational Fluid Dynamics Conference*, pages 649–664, Danvers, Massachusetts, July 1983. AIAA Paper 83-1895-CP.

[8] R. Lehtimäki, A stretching function approach to harmonic grid generation. In *Proceeding of the Second European Computational Fluid Dynamics Conference*, pages 250–257, Stuttgart, 1994.

[9] B.S. Baldwin and H. Lomax, Thin layer approximation and algebraic model for separated turbulent flows, Jan 1978. AIAA Paper 78-257.

[10] K.-Y. Chien, Predictions of channel and boundary-layer flows with a low-Reynods-number turbulence model. *AIAA Journal*, 20(1):33–38, Jan 1982.

[11] W. Kraus, Das MBB-UFE Unterschall-Panel-Verfahren. Teil 3: Flügel-Rumpf-Kombination in kompressibler Strömung. Technical Report MBB-Bericht Nr. UFE 741-71(ö), Messerschmitt-Bölkow-Blohm, 1971.

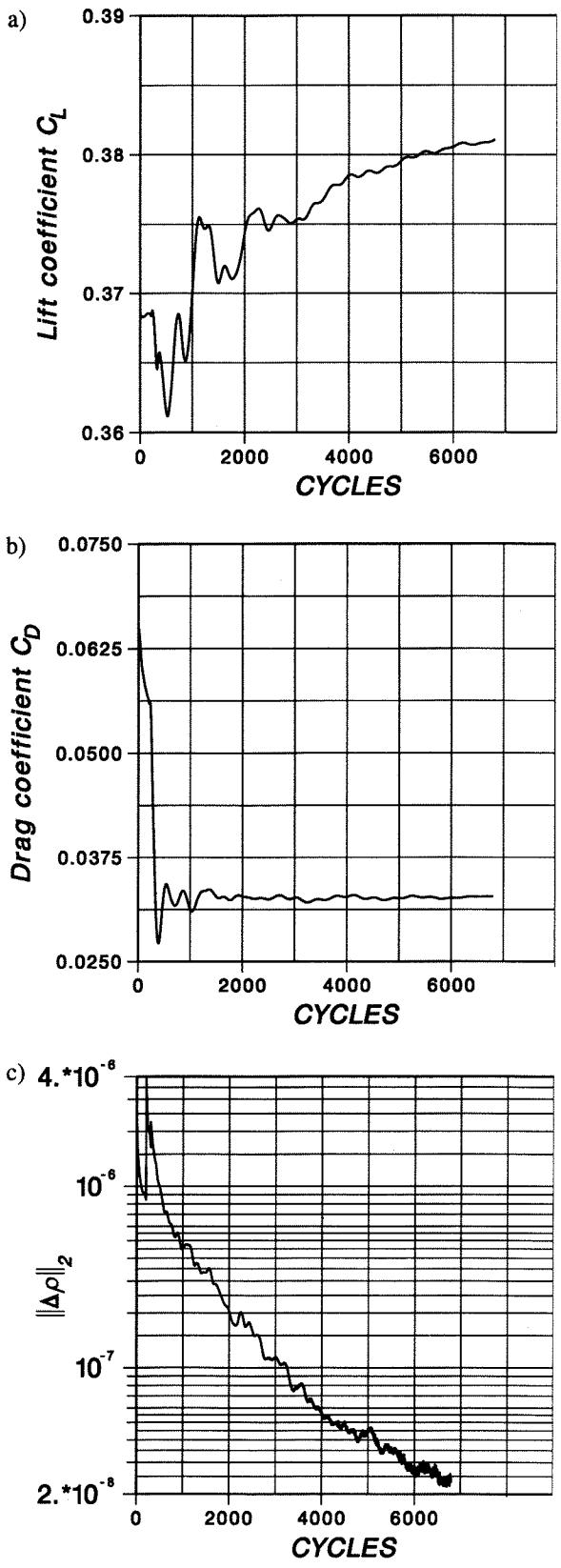

Figure 4. Convergence of the lift and drag coefficients, and the L_2-norm of the density residual for the Baldwin-Lomax turbulence model. $Ma = 0.45$, $Re = 18.6 \times 10^6$, $\alpha = 3°$.

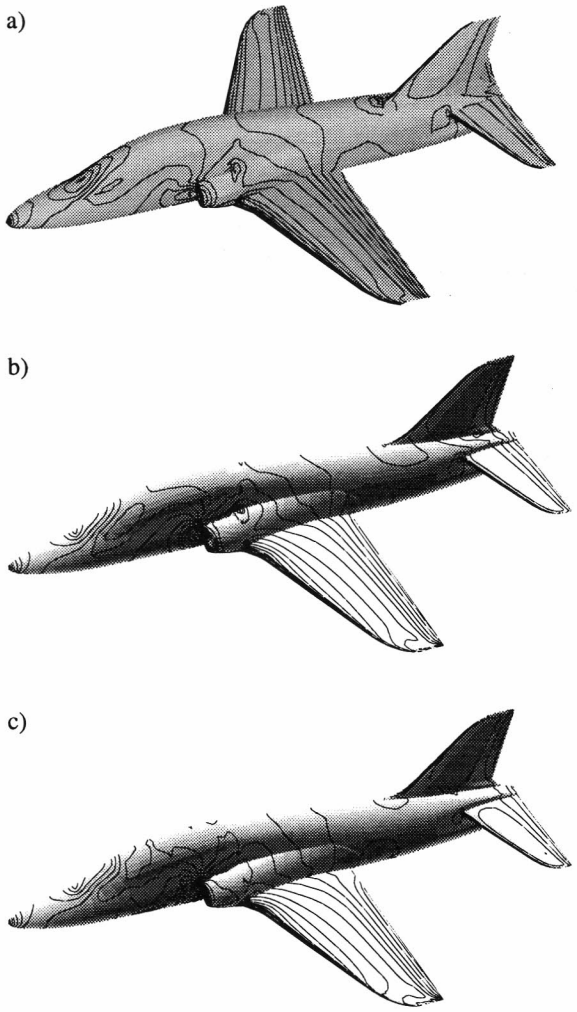

Figure 5. Surface pressure distributions (isobars). $\Delta C_p = 0.1$. Results obtained with a) panel method, b) Baldwin-Lomax turbulence model, c) $k - \epsilon$ model.

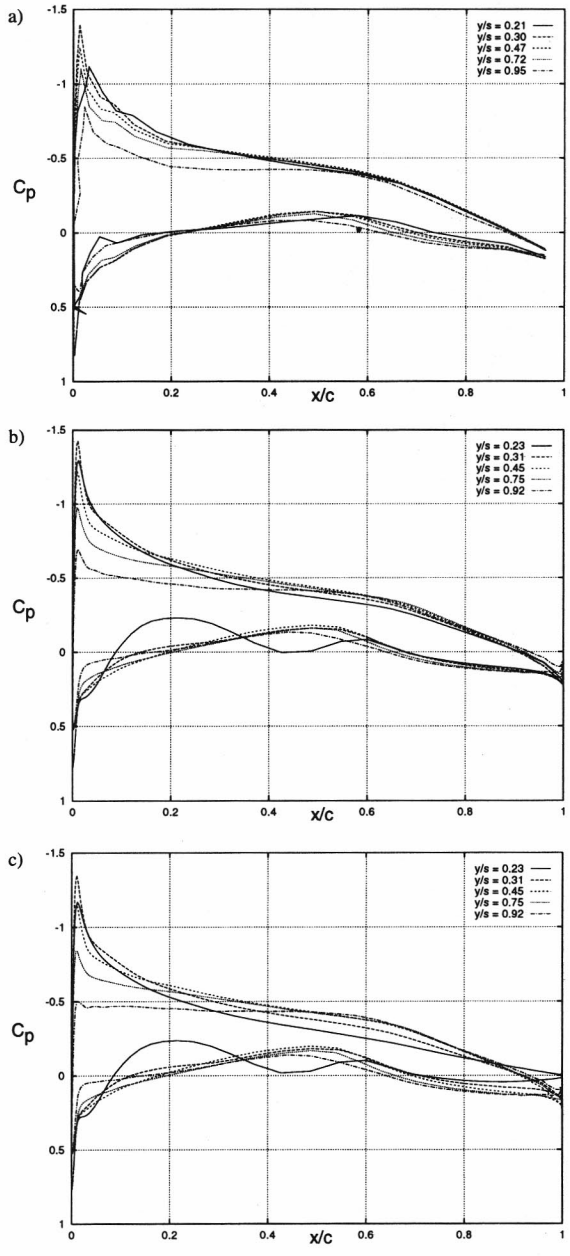

Figure 6. Chordwise pressure coefficient distribution at wing sections $y/s = 0.23$, 0.31, 0.45, 0.75 and 0.92 obtained with a) panel method, b) Baldwin-Lomax turbulence model, c) $k - \epsilon$ model.

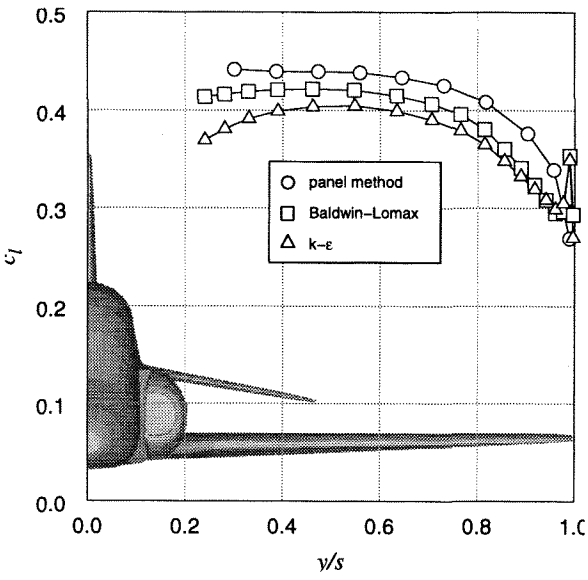

Figure 7. Local lift coefficient c_l of the wing using the Baldwin-Lomax model, the $k-\epsilon$ model and the panel method.

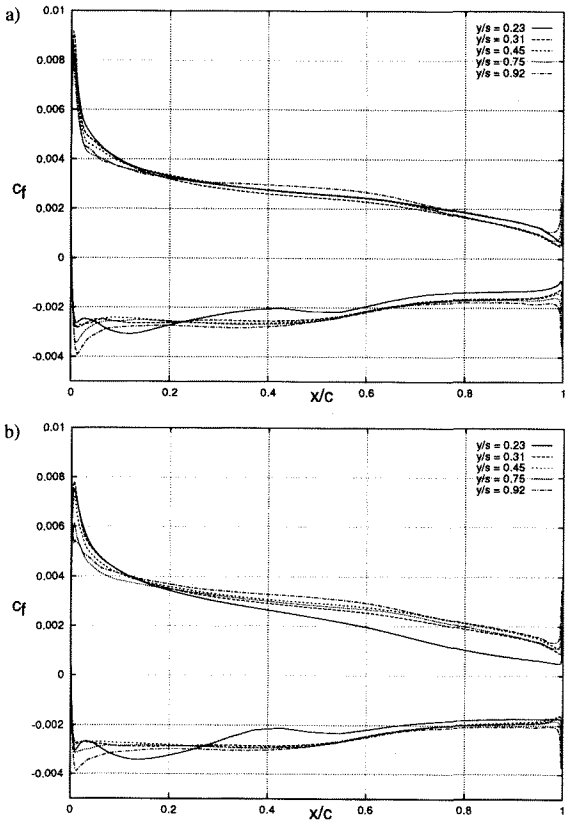

Figure 8. Chordwise friction coefficient c_f at wing sections y/s = 0.23, 0.31, 0.45, 0.75 and 0.92 obtained with a) Baldwin-Lomax model, b) $k-\epsilon$ model.

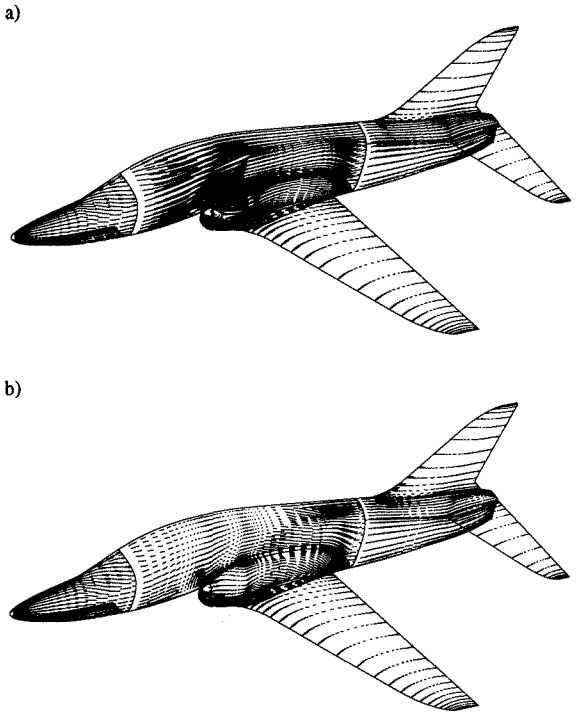

Figure 9. Surface flow distributions as calculated using a) Baldwin-Lomax, b) $k-\epsilon$ model.

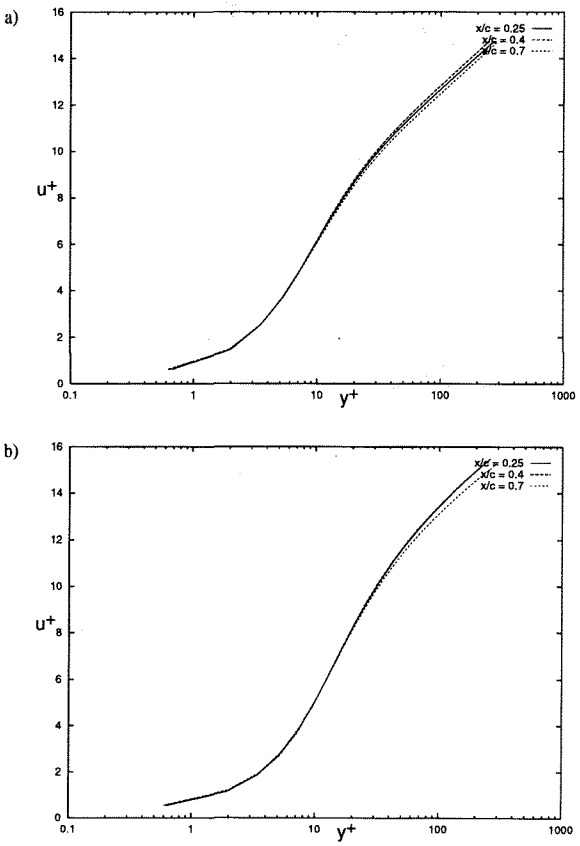

Figure 10. Velocity profiles across the boundary layer of the wing at section y/s=0.45. a) Baldwin-Lomax model, b) $k-\epsilon$ model.